IEEE Access
Multidisciplinary | Rapid Review | Open Access Journal

Received April 24, 2019, accepted May 25, 2019, date of publication June 12, 2019, date of current version July 24, 2019.

Digital Object Identifier 10.1109/ACCESS.2019.2922274

Inductance Characteristic Analysis of Consequent-Pole Permanent Magnet In-Wheel Motor

HUI MA[1], WEIYE WANG[1], XIN QIU[1,2], AND JIANFEI YANG[1,2]
[1]School of Electrical and Automation Engineering, Nanjing Normal University, Nanjing 210046, China
[2]Jiangsu Key Laboratory of 3D Printing Equipment and Manufacturing, Nanjing, 210042, China

Corresponding author: Xin Qiu (qiuxin_nh@163.com)

This work was supported in part by the National Natural Science Foundation of China under Award 51607094 and Award 51407095, in part by the Province Natural Science Foundation of Jiangsu under Project BK20151548, in part by the Jiangsu "Six talent peaks" Project under Project GDZB-043, and in part by the Nanjing Post-Subsidy Program under Project 201722046.

ABSTRACT This paper presents inductance characteristics analysis of the consequent-pole permanent magnet in-wheel motor (CPM). Considering the specialty of consequent-pole structure, this paper analyzes the change rule of the winding self-inductance via equivalent magnetic circuit method (EMCM). The corresponding equivalent resistance is directly given when the rotor is in different positions. Based on this, equivalent magnetic circuit (EMC) that reflects the inductance of the CPM is summarized in this paper. In order to analyze the difference and connection of the inductance among the CPM, two models with 36 slots 32 poles and 48 slots 40 poles are established and compared. Moreover, the Fourier analysis expression of winding self-inductance is deduced to prove the different periodicities of winding self-inductance between two motors. The experimental result is consistent with the theoretical analysis, and the conclusion effectively proves the close relationship between the inductance characteristics and its internal structure of the motor.

INDEX TERMS Consequent-pole, equivalent magnetic circuit method (EMCM), self-inductance, periodicity.

I. INTRODUCTION

In recent years, in-wheel motors have been increasingly used in electric vehicles (EV) which are characterized with simplifying the complex chassis structure, improving the space and energy utilization [1]–[3]. Any type of motors can be made into in-wheel structure, but in contrast, most in-wheel motors use a permanent magnet synchronous motor (PMSM) broadly due to its advantages of high efficiency, high torque density, low torque ripple, and good fault tolerance [4]–[6].

Considering the advantages of direct-drive applications, manufacturing, maintenance and easy installation, the outer rotor with the surface mounted permanent magnet (PM) has been applied into the in-wheel motor. This structure not only consumes more PM materials, but also is poor in field-weakening capacity. However, the PM of common salient-pole motor is designed into '—'-shape and 'V'-shape, which can affect the structural strength of the outer rotor. The outer rotor of salient-pole motor with the '—'-shape PM is relatively thin so it is difficult to form q-axis magnetic circuit with a large inductance, the PM in 'V'-shape is restricted in practical application due to the limit of greater radial length. Under the circumstances, design and placement of PM should be comprehensively considered in order to obtain better motor performance especially reflect in output torque related to motor size and weight and the requirements of the high torque density of the motor [7], [8].

In order to solve these problems, the consequent-pole permanent magnet in-wheel motor (CPM) for EV applications is proposed [9]–[11]. The PM is magnetized radially and uniformly arranged in the middle of the iron pole, the iron is magnetized to the S-pole (N-pole) because magnetic flux-lines circulate between the iron poles and PM, and the PM is magnetized to the N-pole (S-pole) so this kind of motor is called CPM [12], [13]. Compared with traditional PM in-wheel motors, the CPM effectively reduces the cost and broadens the adjustable speed range [14]. CPM with a concentrated winding is conducive to low cogging torque and

The associate editor coordinating the review of this manuscript and approving it for publication was Kan Liu.

enables a significant increase of the inductance to facilitate constant power operation over a wide speed range by flux weakening control [15].

At present, scholars have done a lot of research work on the consequent-pole structure of bearingless permanent magnet motors [16]–[19], but few research work is focused on consequent-pole PMSM. For this reason, research of CPM is necessary and significant. The most prominent performance of the CPM is the flux-weakening capability, and the winding inductance is a key parameter for the flux-weakening capability and can affect the output torque significantly [20]. Hence, the analysis on the characteristic of the winding inductance is very important for the CPM. To analyze the inductance characteristic of the CPM, the essential method is to combine with the internal structure and this is significant to guide the design of the motor. In the initial design of the motor, if the inductance that meets the performance requirements of the motor can be taken into account, the performance of the CPM can be effectively improved and problems will be reduced in the later use of the motor. In addition, the research on inductance can enhance control precision and improve control method. From this perspective, the analysis of the inductance is significant and essential.

The research methods of inductance mainly include the equivalent magnetic circuit method (EMCM), the finite element method (FEM) [21]–[25] and the experimental method [21], [26]–[29]. The EMCM is generally obtained from the magnetic flux-lines distribution analyzed by FEM, and the complexity of the equivalent magnetic circuit (EMC) will change with different operating conditions and consideration factors. Due to the particularity of the consequent-pole structure, the equivalent air gap distribution of the CPM is uneven and the resistance of the air gap changes with the rotor position changing. This condition causes the EMC of the CPM to become complicated and different from others, hence analysis in the CPM should be reconsidered. Based on the complex structure of the motor, the FEM is usually time-consuming. Although it can directly offer the results, it cannot demonstrate the relationship between the motor inductance characteristic and the internal structure. The experimental method can get the required data by creating external conditions, but it still can't figure out the internal mechanism of the CPM. This makes it a difficult and important point to study the inductance from the internal structure of the CPM. Based on the analyzed above, the inductance of the CPM is necessary to be studied from its internal structure.

In this paper, two models with different slot-pole numbers matching are established and compared. Focusing on the internal structure of the CPM, the characteristic of the inductance are studied by FEM and EMCM. Furthermore, EMC suitable for the structure of the CPM is established with the change of the rotor position. In order to explain the reason for the inductance showing different periodicities between two motors, the connections and differences about the internal structures are illustrated. Finally, the experimental result and theoretical analysis are consistent.

II. COMPARISON BETWEEN THE CONVENTIONAL IN-WHEEL MOTOR AND CPM

The structures of the conventional direct-drive permanent magnet in-wheel motor and consequent-pole permanent magnet in-wheel motor are shown in Fig. 1. Two models both consist of a stator and a rotor, the stator is composed of iron core and windings, the rotor is composed of iron core and permanent magnetic steel. The stator is located inside the rotor, and the permanent magnet steel is placed inside the rotor to achieve direct-drive in-wheel applications [30].

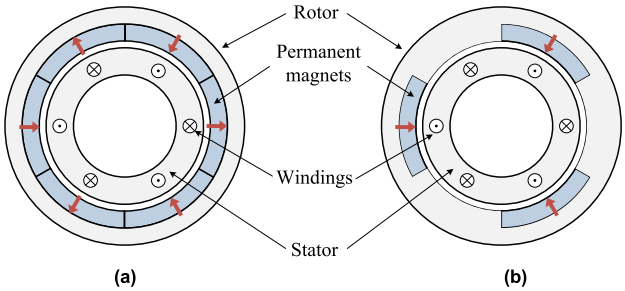

FIGURE 1. The structures of the conventional direct-drive permanent magnet in-wheel motor and consequent-pole permanent magnet in-wheel motor.

Compare Fig. 1 (a) with (b), polarity of the permanent magnet steel in Fig. 1 (a) is alternately distributed in N-S-N manner. Because the number of permanent magnetic steel for the consequent-pole permanent magnet in-wheel motor in Fig. 1 (b) is reduced by half and the magnetic steel is replaced with silicon steel, the rest of the magnetic steel is distributed in an N-N or S-S manner [31]. Under this circumstance, the silicon steel teeth produce a magnetic pole which is contrary to the polarity of permanent magnetic steel, hence the basic polarity requirements of motor operation can be met. At the same time, it causes the unevenness of the equivalent air gap, in order to satisfy the requirement of air gap, the volume of magnetic steel must be increased. As a result, the EMC of conventional in-wheel motors is mainly composed of magnetic steel and air gap, while the EMC of the CPM is alternating between magnetic steel and silicon steel. The resistance distribution and the equivalent resistance are constantly changing as the rotor rotates, which causes the variation of the inductance. This situation makes it difficult to analyze the inductance of the CPM. Therefore, the conventional EMCM is not suitable for the CPM, but inductance of the CPM also follows a certain rule. In order to promote the optimization and application of the CPM, it is necessary to analyze its inductance rules from its internal structure.

III. MODELING OF THE CPM

In order to analyze the inductance related to its internal structure of the CPM, two models with different slot-pole numbers matching are established in Fig. 2. Both types of motors are distributed by a concentrated winding. Because of the 3-phase symmetry, inductance of one-phase winding taken as an example is analyzed in this paper.

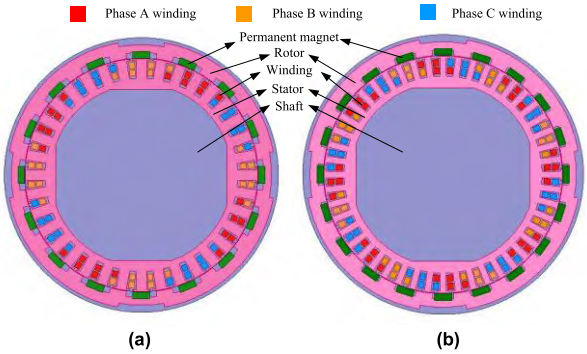

FIGURE 2. The structure of two models. (a) 36 slots 32 poles. (b) 48 slots 40 poles.

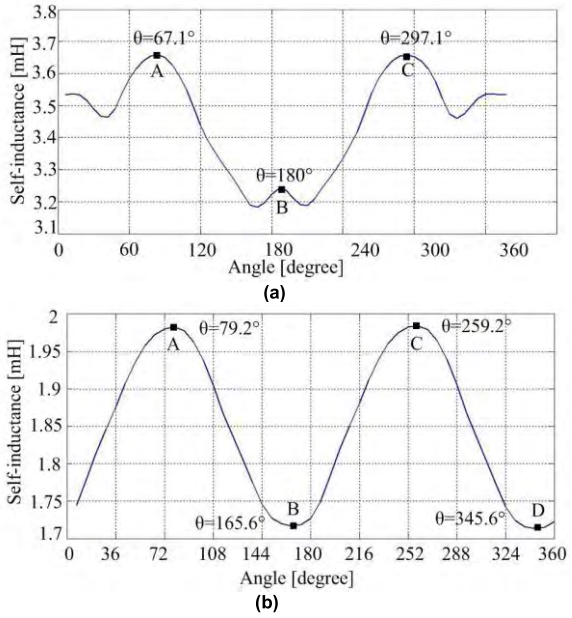

FIGURE 3. Winding self-inductance of two motors. (a) 36 slots 32 poles. (b) 48 slots 40 poles.

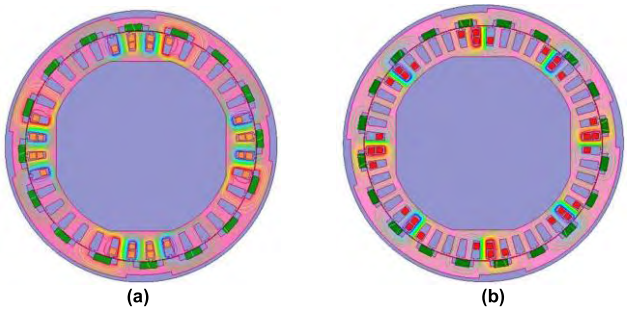

FIGURE 4. Flux-lines distributions of two motors. (a) 36 slots 32 poles. (b) 48 slots 40 poles.

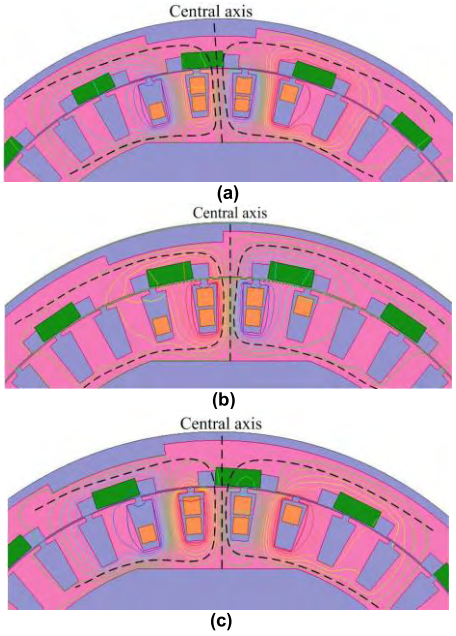

FIGURE 5. FEA of the 36 slots 32 poles motor in (a) $\theta = 67.1°$, (b) $\theta = 180°$ and (c) $\theta = 297.1°$.

As shown in Fig. 2, the CPM system is symmetric and the unit motor of two models are chosen to be modeled. Their self-inductances analyzed by FEM in an electric period are shown in Fig. 3, separately.

Compared Fig. 3 (a) with (b), the inductance of the 48 slots 40 poles motor shows better sinusoidal property than that of the 36 slots 32 poles motor. In particular, the inductance of the former has only one period (called unipolar) while that of the latter has two periods (called bipolar) in one electric cycle. In order to analyze the relationship between the motor structure and inductance, this paper analyzes the cause of inductance from the distribution of flux-lines, PM and stator winding. The corresponding EMC is established and the magnetoresistance expression of the corresponding position is summarized.

A. ANALYSIS OF THE DISTRIBUTION OF FLUX-LINES INFLUENCED ON THE INDUCTANCE

It is well known that there is a certain relationship between flux-lines and inductance. Inductance is not convenient for direct observation, but the flux-linkage is the opposite. The distribution of flux-lines varies according to the distribution of PM, windings, etc. Therefore, it is feasible to study the distribution of flux-lines firstly and explore the relationship between its distribution and the internal structure of the motor.

Fig. 4 (a) and (b) show the flux-lines distributions of two motors respectively. It can be seen that the flux-lines present periodicity due to the distribution of concentrated winding. In order to simplify the model analysis and calculation, quarter and eighth of the two models are simulated respectively. Fig. 5 and 6 show the results of the FEM.

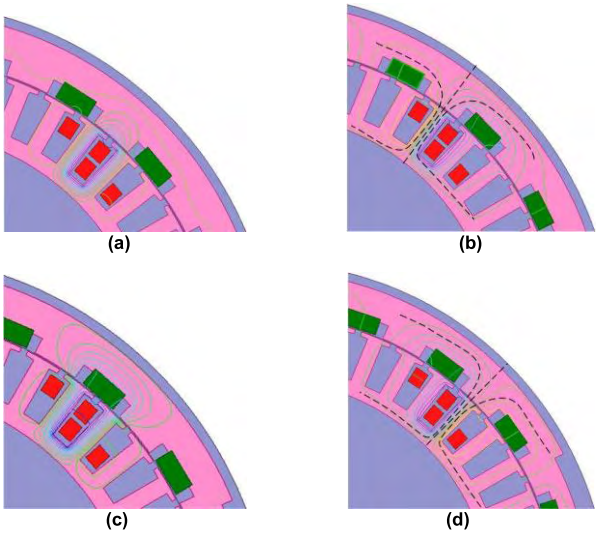

FIGURE 6. FEA of the 48 slots 40 poles motor in (a) $\theta = 79.2°$, (b) $\theta = 165.6°$, (c) $\theta = 259.2°$ and (d) $\theta = 345.6°$.

In order to analyze the inductance characteristics, this paper selects the maximum and minimum values of the self-inductance of each motor, and the FEM corresponded to the points marked in Fig. 3 is shown in Fig. 5 and 6. In Fig. 5, the self-inductance of the 36 slots 32 poles motor is at maximum when $\theta = 67.1°$ or 297.1°, part of the flux-lines pass through the PM and form magnetic circuits with the stator slot, the other part of the flux-lines form the magnetic circuits among the rotor core, air gap and stator slots. When $\theta = 180°$ the self-inductance of the motor is at minimum, most of the flux-lines form the magnetic circuits among the rotor core, air gap and stator slots. The common point of the magnetic circuits are axially symmetric about the central axis. In Fig. 6, the self-inductance of the 48 slots 40 poles motor is at maximum when $\theta = 79.2°$ or 259.2°, the flux-lines mainly pass through the rotor core, air gap and stator slots and there's only one type of magnetic circuits. However, when $\theta = 165.6°$ or 345.6° the self-inductance of the motor is at minimum, the flux-lines form two parts of magnetic circuits and magnetic circuits is mirror symmetry when $\theta = 165.6°$ or 345.6°.

It can be known from the above analysis, for one CPM, when the inductance value is at the maximum or minimum, the distribution of flux-lines has the same feature. Due to the different slot-pole numbers matching, the distribution of flux-lines between the two motors is different. In addition, the distribution of flux-lines about 36 slots 32 poles changes twice and that of 48 slots 40 poles changes once in an electric cycle. This is similar to the rule of inductance change in an electric cycle.

B. ANALYSIS OF THE INDUCTANCE CHARACTERISTIC FROM EMC

In order to directly analyze the law of inductance change, the magnetic circuit is simplified and quantitatively analyzed by the EMCM. As can be seen from the flux-lines distribution shown in Fig. 5 and 6, the main EMC includes the rotor yoke, rotor tooth, air gap, stator tooth and stator yoke. In addition, part of the EMC passes through the PM and the magnetoresistance of PM is considered. The permeances of the ferromagnetic regions and the PM are relatively easy to determine, but the calculations for the permeances of the airgap region are more complicated. Thus, to simplify calculations, the flux paths between the CPM's stator and rotor are simplified and the saturation effect is neglected in the process of calculation. Three kinds of magnetoresistances in main magnetic circuit are shown in Fig. 7.

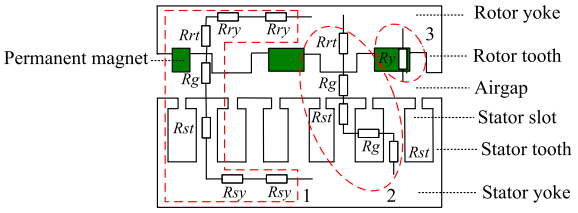

FIGURE 7. Partial magnetoresistance in main magnetic circuit.

The symbols in Fig. 7 represent the following:

R_{ry} Ferromagnetic resistance of rotor yoke
R_{sy} Ferromagnetic resistance of stator yoke
R_{rt} Ferromagnetic resistance of rotor tooth
R_{st} Ferromagnetic resistance of stator tooth
R_g Gap resistance between rotor and stator
R_y Internal magnetoresistance of PM

Based on what have been analyzed above, Fig. 8 and 9 show the corresponding EMC (as the points marked in Fig. 3) respectively.

In Fig. 8 and 9, F_m is the magnetic potential of a single winding.

Observing the EMC related to the distribution of flux-lines, the magnetoresistance of the 36 slots 32 poles motor changes once and that of 48 slots 40 poles motor changes twice in one electric cycle. The basic equation to calculate winding self-inductance of each EMC model is given by

$$L = \frac{N^2}{R} \tag{1}$$

where L, N, and R is self-inductance, number of winding turns, and total magnetoresistance of EMC respectively.

To facilitate the analysis, the following assumptions are made:

(1) The magnetic permeability of the core is infinite, and the magnetic potential of stator and rotor core is the same;

(2) The permeability of the PM is approximately equal to that of air;

(3) Ignore the effect of a small amount of magnetic leakage.

According to the principle of series and parallel magnetoresistance, the total magnetoresistance of each EMC is calculated separately:

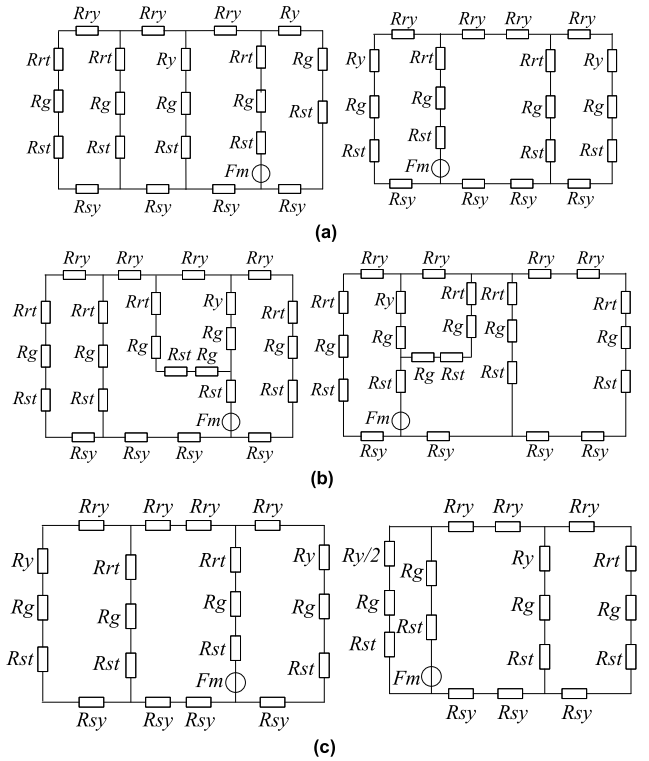

FIGURE 8. EMC of the 36 slots 32 poles motor in (a) $\theta = 67.1°$, (b) $\theta = 180°$ and (c) $\theta = 297.1°$.

In Fig. 7:

$$R_a = \frac{1}{\frac{3}{R_g}+\frac{1}{R_g+R_y}}+R_g+\frac{1}{\frac{2}{R_g+R_y}+\frac{1}{R_g}}+R_g \tag{2}$$

$$R_b = 2\left(\frac{R_g}{3}+\frac{1}{\frac{1}{2R_g}+\frac{1}{R_g+R_y}}\right) \tag{3}$$

$$R_c = \frac{1}{\frac{2}{R_g+R_y}+\frac{1}{R_g}}+R_g+\frac{1}{\frac{1}{R_g+\frac{R_y}{2}}+\frac{1}{R_g+R_y}+\frac{1}{R_g}}+R_g \tag{4}$$

In the process of magnetic circuit simplification, it is noticed that part of the branch in Fig. 8 (b) is shown in circuit 2 in Fig. 7. When the loop passes through the stator slot, the gap resistance is much larger than that between the stator and rotor, therefore in the calculation of formula (3), the magnetic conductance of that part can be equivalent to 0.

Because the permeability of the PM is approximately equal to that of air, the magnetoresistance of the PM can be equivalent to the air-gap. Equation (2)-(4) can be simplified as follows:

$$R_a = \frac{1}{\frac{3}{R_g}+\frac{1}{R_g+R_g}}+R_g+\frac{1}{\frac{2}{R_g+R_g}+\frac{1}{R_g}}+R_g = \frac{39}{14}R_g \tag{5}$$

$$R_b = 2\left(\frac{R_g}{3}+\frac{1}{\frac{1}{R_g+R_g}}\right) = \frac{14}{3}R_g \tag{6}$$

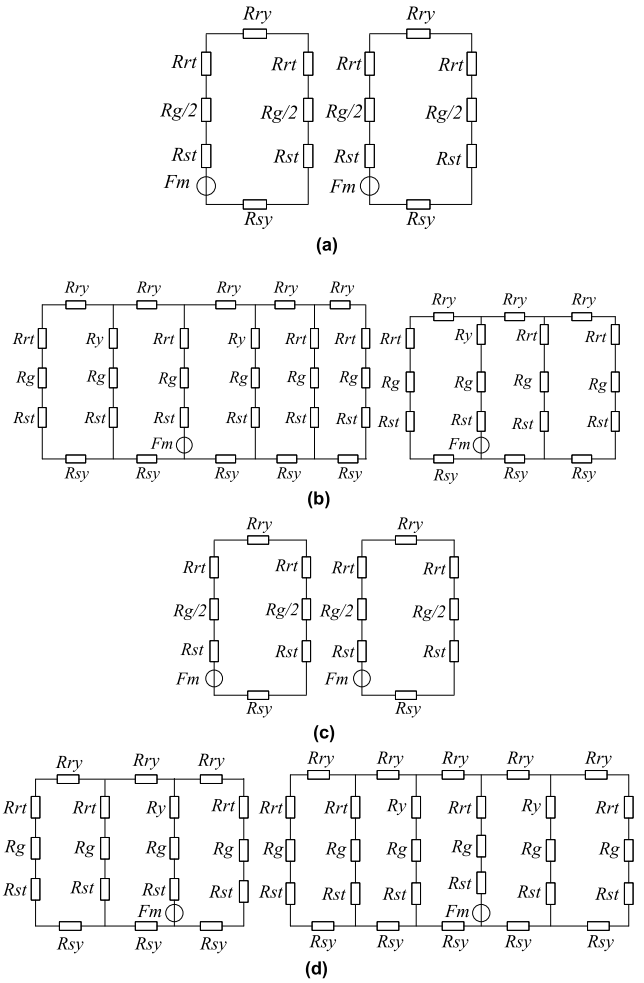

FIGURE 9. EMC of the 48 slots 40 poles motor in (a) $\theta = 79.2°$, (b) $\theta = 165.6°$, (c) $\theta = 259.2°$ and (d) $\theta = 345.6°$.

$$R_c = \frac{1}{\frac{2}{R_g+R_g}+\frac{1}{R_g}}+R_g+\frac{1}{\frac{1}{R_g+\frac{R_g}{2}}+\frac{1}{R_g+R_g}+\frac{1}{R_g}}+R_g = \frac{77}{26}R_g \tag{7}$$

In Fig. 8:

$$R_a = 2R_g = R_c \tag{8}$$

$$R_b = \frac{1}{\frac{3}{R_g}+\frac{2}{R_g+R_y}}+R_g+\frac{R_g}{3}+R_y+R_g = R_d \tag{9}$$

Similarly, equation (9) can be simplified as follows:

$$R_b = \frac{1}{\frac{3}{R_g}+\frac{2}{R_g+R_g}}+R_g+\frac{R_g}{3}+R_g+R_g = \frac{43}{12}R_g = R_d \tag{10}$$

where R_i ($i = a, b, c, d$) represents the total magnetoresistance of EMC in the Fig. 8 and 9.

Due to the irregular distribution of flux-lines during the rotation, the magnetoresistance in the air-gap is constantly changing, so the magnetoresistance of the air-gap cannot be accurately calculated. Therefore, it is simplified to represent the air-gap magnetoresistance. Combined with the

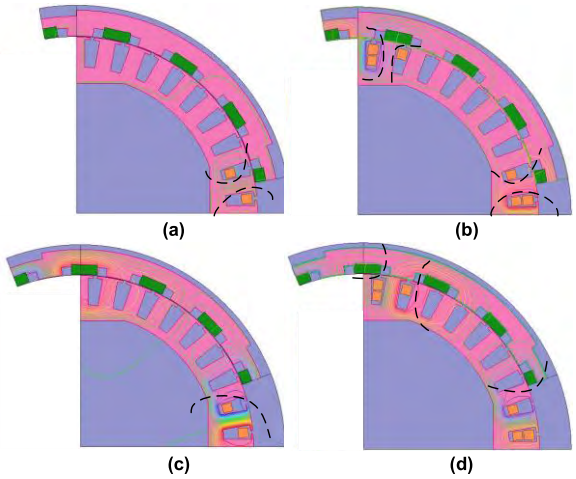

FIGURE 10. Inductance analyzed by FEM of the 36 slots 32 poles motor. (a) Inductance at its minimum when the motor has only one set of coils. (b) Inductance at its minimum when the motor has coils in series. (c) Inductance at its maximum when the motor has only one set of coils. (d) Inductance at its maximum when the motor has coils in series.

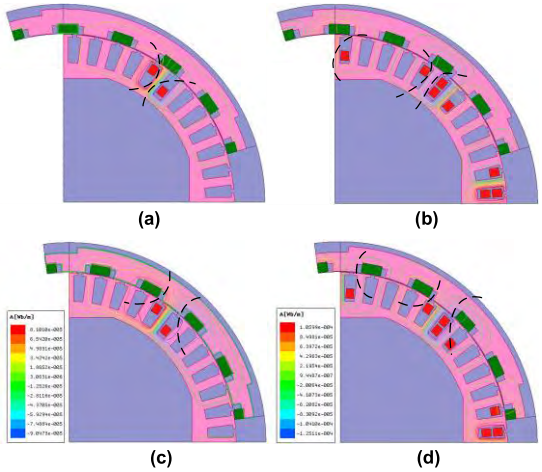

FIGURE 11. Inductance analyzed by FEM of the 48 slots 40 poles motor. (a) Inductance at its minimum when the motor has only one set of coils. (b) Inductance at its minimum when the motor has coils in series. (c) Inductance at its maximum when the motor has only one set of coils. (d) Inductance at its maximum when the motor has coils in series.

equation (5)-(7), $R_a < R_b$, $R_c < R_b$, although R_a and R_c are not exactly equal, the difference is within acceptable limits because the actual inductance values are not exactly equal. In the same way, compared with equation (8) and (10), $R_b = R_d < R_a = R_c$. According to equation (1), the corresponding relationship between the inductance and magnetoresistance can be concluded clearly. When the inductance of the motor is at maximum, the total magnetoresistance is at minimum. Similarly, when the inductance of the motor is at minimum, the total magnetoresistance is at maximum. Therefore, it is feasible to calculate the inductance with the rotor in any position and analyze the inductance characteristic of the motor by using EMCM.

C. ANALYSIS OF THE DISTRIBUTION OF PM AND STATOR WINDING INFLUENCED ON THE INDUCTANCE

The inductance periodicities of the two motors are different as can be seen from Fig. 3, the distribution of flux-lines and the magnetoresistance show that the inductance of the two motors changes once and twice respectively. But in order to study the relation between the inductance and the internal structure of the motor, coil windings of the two motors are compared and analyzed in the following.

The winding self-inductance of the two motors is shown in Fig. 3, the inductance of 36 slots 32 poles motor has one period, while that of 48 slots 40 poles motors has two. In order to analyze the cause of inductance of two motors, finite element analysis (FEA) of one coil and one-unit motor are carried out in Fig. 10 and 11, the inductance waveform is shown in Fig. 12.

Observing the distribution of the PM, stator core and winding, it is intuitively to be seen from Fig. (a) and (c) in Fig. 10 and 11, when the inductance is at the minimum, the PM is between one coils of the windings. When the

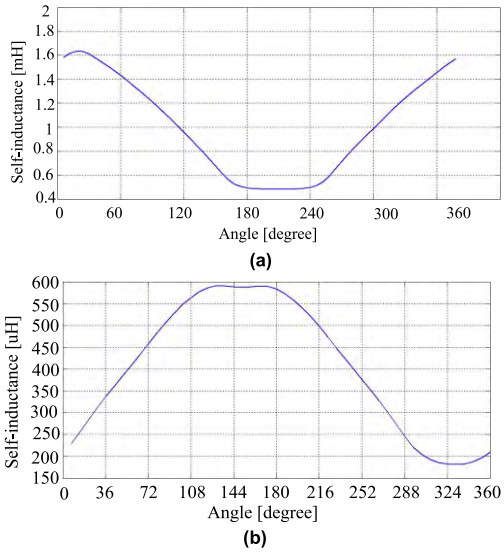

FIGURE 12. Inductance of one coil of phase windings. (a) 36 slots 32 poles. (b) 48 slots 40 poles.

inductance is at its maximum, the PM is located on both sides of one coil about the windings. Fig. (b) and (d) in Fig. 10 and 11 show that windings of one-unit motor satisfy this rule.

From Fig. 12, the one coil self-inductance of two motors present the characteristics of unipolar. The one-phase winding is composed of coils in series and the inductance of phase winding is superimposed by inductance of multiple coils, so the inductance of one coil is analyzed. Fourier analysis is used to explore the reasons for unipolar and bipolar of the inductance of one-phase winding.

As can be seen from Fig. 13 (a), inductance of per coil and one phase of 36 slots 32 poles motor both contain many harmonics, and the self-inductance of per coil

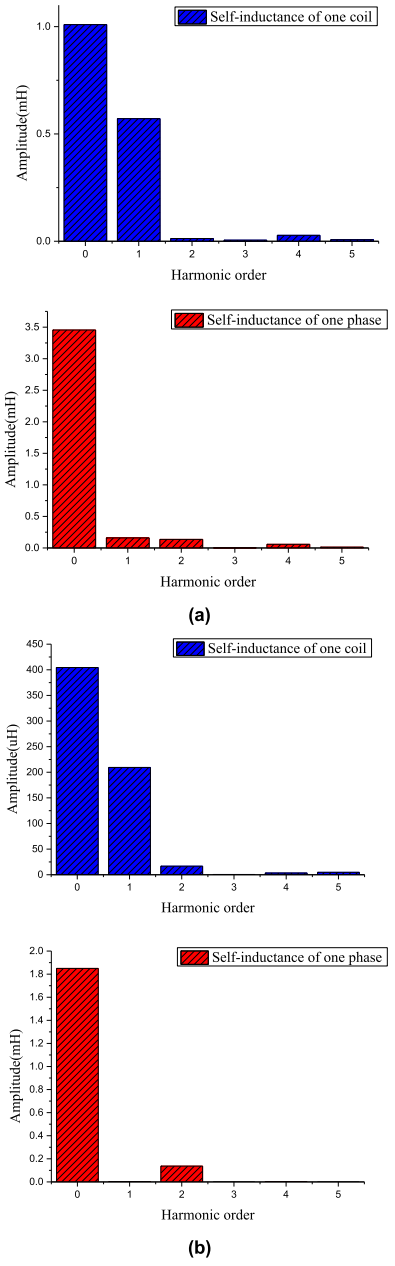

FIGURE 13. Fourier analysis of self-inductance about one coil and one phase. (a) 36 slots 32 poles. (b) 48 slots 40 poles.

contains first harmonic. The self-inductance of one phase mainly includes first and second harmonics, and the amplitude of the first harmonic is greater than that of the second harmonic. Combined with Fig. 3 (a), the minimum of self-induction occurs only once, but the change between the maximum and minimum occurs twice. It is also found that the self-inductance waveform is symmetric about the minimum point. Therefore, both the first and second harmonics play a role, the first harmonic ultimately make the self-inductance unipolar. The inductance of per coils and one phase of a 48 slots 40 poles motor mainly include the first and second harmonic respectively. The inductance of per coil is expressed by Fourier series, and then the phase self-inductance is added up by inductance of all coils.

To simplify the calculation, the first, second and third harmonics are taken into consideration, ignoring the higher harmonics. The inductance of per coil and one phase of two motors are expressed as follows.

In the 36 slots 32 poles motor:

$$L_{(1)} = L_0 + L_1\cos(\omega t) + L_2\cos(2\omega t + 20^\circ) + L_3\cos(3\omega t + 40^\circ) + \cdots \quad (11)$$

$$L_{(2)} = L_0 + L_1\cos(\omega t - 40^\circ) + L_2\cos(2\omega t + 60^\circ) + \cdots \quad (12)$$

$$L_{(3)} = L_0 + L_1\cos(\omega t - 20^\circ) + L_2\cos(2\omega t - 20^\circ) + \cdots \quad (13)$$

$$\begin{aligned} L_a &= L_{(1)} + L_{(2)} + L_{(3)} \\ &= 3L_0 + L_{11}\cos(\omega t) - L_{12}\sin(\omega t) + L_{21}\cos(2\omega t) \\ &\quad - L_{22}\sin(2\omega t) + \cdots \end{aligned} \quad (14)$$

In the 48 slots 40 poles motor:

$$L_{(1)} = L_0 + L_1\cos(\omega t) + L_2\cos(2\omega t) - L_3\cos(3\omega t) + \cdots \quad (15)$$

$$L_{(2)} = L_0 - L_1\cos(\omega t + 30^\circ) + L_2\cos(2\omega t + 60^\circ) + \cdots \quad (16)$$

$$L_{(3)} = L_0 + L_1\cos(\omega t + 30^\circ) + L_2\cos(2\omega t + 60^\circ) + \cdots \quad (17)$$

$$L_{(4)} = L_0 - L_1\cos(\omega t) + L_2\cos(2\omega t) + \cdots \quad (18)$$

$$\begin{aligned} L_a &= L_{(1)} + L_{(2)} + L_{(3)} + L_{(4)} \\ &= 3L_0 + 3L_{21}\cos(2\omega t) - \sqrt{3}L_{22}\sin(2\omega t) + \cdots \end{aligned} \quad (19)$$

The symbols in equation (11)-(19) represent the following:

$L_{(1)}, L_{(2)}, L_{(3)}, L_{(4)}$ Inductance of per coil

L_0, L_1, L_2, L_3 Fundamental wave, coefficient of first, second and third harmonic

L_{11}, L_{12} Coefficient of first harmonic after the superposition

L_{21}, L_{22} Coefficient of second harmonic after the superposition

ω Angular velocity of motor rotation

From equation (14), the inductance of A-phase winding in the 36 slots 32 poles motor carries the first and second harmonics, and the Fourier analysis data shows that the first and second harmonic coefficients are 0.159046 and 0.135567 respectively. In contrast, the first harmonic has a larger effect, and finally the phase self-inductance presents unipolar. At the same time, self-inductance waveform has some symmetry because of the second harmonic. Equation (19) shows that the winding inductance of the 48 slots 40 poles motor only has the second harmonic after superposition, and then inductance presents bipolar.

D. SUMMARY OF THE INDUCTANCE ABOUT THE CPM

Based on the analysis in section A, B and C, due to the periodicity of the inductance, when the inductance is at the

maximum or minimum value, the distribution of flux-lines presents the same or mirror symmetry. So are the EMC of the CPM. In addition, when the inductance is at the maximum, the PM are distributed on both sides of the coil. When the inductance is at the minimum, the PM is in the middle of the coil. Based on the series winding, the inductance of the CPM is superposed by the coil inductance and finally presents different periodicities. This method is suitable for the CPM with different slot-pole numbers matching, and the inductance of one-coil winding can be analyzed to study the periodicity of the CPM. Furthermore, the inductance in any position can be calculated by EMCM and the calculation results provide the basis for the motor in the initial design stage.

IV. EXPERIMENTAL VERIFICATION

The previous sections fully prove the relationship between the inductance characteristic and the structure of the CPM through a large number of simulations and calculations. But there is no way to observe the internal structure of the CPM from the outside and measure the winding self-inductance directly. To verify the inductance characteristic of the motor, this paper calculates the phase-inductance based on the FEM. Then the phase-inductance measured by the experiment is compared with the calculated result. The relationship exists between the self-inductance and phase-inductance according to the expression [32]:

$$L_a = \frac{3}{2}L_{aa} - 3L_{s2}\cos^2\theta + \frac{\varphi_f \cos\theta}{i_a} \tag{20}$$

where $L_{s2} = \frac{1}{2}\left(L_{AAq} - L_{AAd}\right)$

L_a The phase-inductance of stator windings

L_{aa} The self-inductance between stator windings

θ Electrical angle of the rotor

L_{AAq} The equivalent of q axis inductance of stator windings of A-phase

L_{AAd} The equivalent of d axis inductance of stator windings of A-phase

φ_f The flux linkage due to the PM

i_a Current of A-phase

The variables in the formula (20) are all obtained by FEM. In order to reduce the error, the phase current is extremely small. Therefore, the error of the value of phase-inductance obtained by FEM is generally small.

Fig. 14 shows two prototypes to investigate and verify the characteristic of the mentioned CPM. Table 1 lists the same structural parameters of the two experimental prototypes. The differences between two motors are that the magnet steel length is 10.56 mm and 13.2 mm, and the number of turns per slot in series is 26 and 15 respectively.

The experiments on the CPM are performed in the environment as shown in Fig. 15. The servo motor (MDME302GCGM) is connected to the test motor through a coupling, and the servo controller (MFDKTA390CA1) is used to rotate the servo motor in order to change the position of the test motor. The neutral line of the motor is drawn out and the phase-inductance can be directly measured by LCR Meter (HIOKI IM 3533-01).

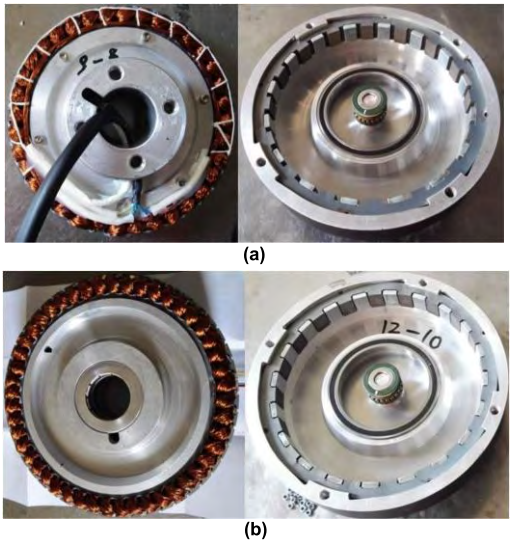

FIGURE 14. Prototype of two motors. (a) 36 slots 32 poles. (b) 48 slots 40 poles.

TABLE 1. Structure parameters of the experimental prototype.

Parameters	value	Parameters	value
Outer diameter of the stator	89mm	Outer diameter of the rotor	89.5mm
Inner diameter of the stator	69.5mm	Inner diameter of the rotor	102.5mm
Stator slot width	2mm	Thickness of the magnet steel	5mm
Length of air gap	0.5mm	Axis length of iron core	26mm
Rated power	300W	Rated speed	300rpm
Rated torque	10N·m	Rated phase current	10A
Bus voltage	48V		

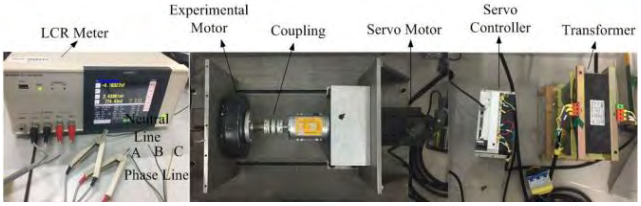

FIGURE 15. The experiment platform.

Based on this, the actual phase-inductance of two motors are finally measured when the output frequency is 300Hz. The results of the wingding phase-inductance calculated and measured are compared.

It can be seen from the Fig. 16 that both the calculated and measured phase-inductance values have the same change rule. Due to the rotor position control is not particularly accurate, and there are some errors in the actual processing, there is a certain deviation. But the periodicity is completely consistent with the calculated. The phase-inductance of the 36 slots 32 poles motor calculated is consistent with

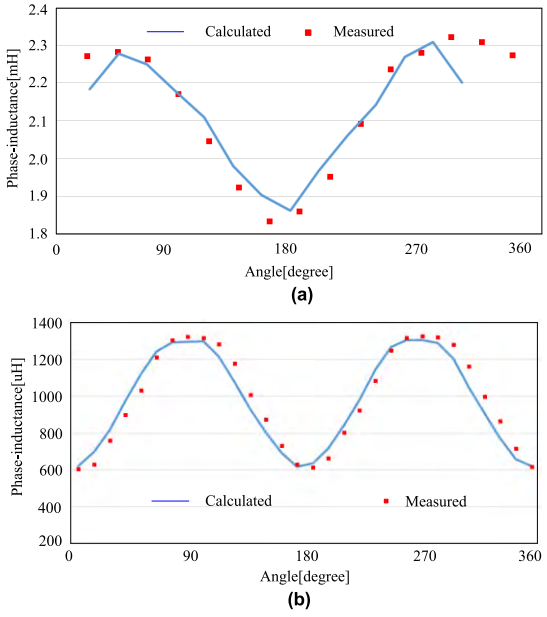

FIGURE 16. Winding phase-inductance are calculated and measured of the CPM. (a) 36 slots 32 poles. (b) 48 slots 40 poles.

the measured and the inductance shows unipolar. Phase-inductance of the 48 slots 40 poles motor calculated is much well the same as the measured and the inductance shows bipolar.

V. CONCLUSION

Based on the two consequent-pole PMSM motors of different pole-slot combinations, although the slot-pole numbers matching are not the same, the relationship between the characteristics of the inductance and the internal structure is the same. In particular, it is reflected the distribution of the magnetic circuit and the relationship between the PM and the winding. However, due to the different distributions of windings, the superposition results of the inductance of two motor are different. Considering the series-parallel winding, this paper analyzes the inductance of one coil and one-unit in two motors by FFT. The Fourier analysis expression of winding self-inductance is deduced to prove the different periodicity of winding self-inductance between two models. Experimental results and theoretical analysis are consistent, and the conclusion effectively proves the close relationship between the inductance characteristics and its internal structure of the motor.

REFERENCES

[1] Z. Liu, W. Zhao, and J. Ji, "Electromagnetic performance of double-stator flux-modulation permanent-magnet motor," *IEEE Trans. Appl. Supercond.*, vol. 26, no. 4, Jun. 2016, Art. no. 5205205.

[2] K. Sone, M. Takemoto, S. Ogasawara, K. Takezaki, and H. Akiyama, "A ferrite PM in-wheel motor without rare earth materials for electric city commuters," *IEEE Trans. Magn.*, vol. 48, no. 11, pp. 2961–2964, Nov. 2012

[3] A. Masmoudi and Z.-Q. Zhu, "Fractional slot permanent magnet brushless machines and drives for electric and hybrid propulsion systems," *COMPEL- Int. J. Comput. Math. Elect. Electron. Eng.*, vol. 30, no. 1, pp. 9–31, 2011.

[4] A. M. EL-Refaie, "Fractional-slot concentrated-windings synchronous permanent magnet machines: Opportunities and challenges," *IEEE Trans. Ind. Electron.*, vol. 57, no. 1, pp. 107–121, Jan. 2010.

[5] U.-J. Seo, Y.-D. Chun, J.-H. Choi, S.-U. Chung, P.-W. Han, and D.-H. Koo, "General characteristic of fractional slot double layer concentrated winding synchronous machine," *J. Elect. Eng. Technol.*, vol. 8, no. 2, pp. 282–287, Mar. 2013.

[6] N. Bianchi, S. Bolognani, M. D. Pre, and G. Grezzani, "Design considerations for fractional-slot winding configurations of synchronous machines," *IEEE Trans. Ind. Appl.*, vol. 42, no. 4, pp. 997–1006, Jul./Aug. 2006.

[7] C. J. Ifedi, B. C. Mecrow, S. T. M. Brockway, G. S. Boast, G. J. Atkinson, and D. Kostic-Perovic, "Fault-tolerant in-wheel motor topologies for high-performance electric vehicles," *IEEE Trans. Ind. Appl.*, vol. 49, no. 3, pp. 1249–1257, May/Jun. 2013.

[8] J. Li, J. Wang, Z. Zhigang, and W. Yan, "Analytical analysis and implementation of a low-speed high-torque permanent magnet vernier in-wheel motor for electric vehicle," *J. Appl. Phys.*, vol. 111, no. 7, Mar. 2012, Art. no. 07E727.

[9] T. Takenaga, Y. Kubota, A. Chiba, and T. Fukao, "A principle and winding design of consequent-pole bearingless motors," *JSME Int. J. C, Mech. Syst., Mach. Elements Manuf.*, vol. 46, no. 2, pp. 363–369, 2003.

[10] H. Sugimoto, K. Kamiya, R. Nakamura, J. Asama, A. Chiba, and T. Fukao, "Design and basic characteristics of multi-consequent-pole bearingless motor with bi-tooth main poles," *IEEE Trans. Magn.*, vol. 45, no. 6, pp. 2791–2794, Jun. 2009.

[11] T. Takenaga, Y. Kubota, A. Chiba, and T. Fukao, "A principle and a design of a consequent-pole bearingless motor," in *Proc. 8th Int. Symp. Magn. Bearing*, Mito, Japan, Aug. 2002, pp. 259–264.

[12] J. R. Hendershot, Jr., and T. J. E. Miller, *Design of Brushless Permanent-Magnet Motors*. New York, NY, USA: Oxford, 1994.

[13] J. Amemiya, A. Chiba, D. G. Dorrell, and T. Fukao, "Basic characteristics of a consequent-pole-type bearingless motor," *IEEE Trans. Magn.*, vol. 41, no. 1, pp. 82–89, Jan. 2005.

[14] S.-U. Chung, S.-H. Moon, D.-J. Kim, and J.-M. Kim, "Development of a 20-pole–24-slot SPMSM with consequent pole rotor for in-wheel direct drive," *IEEE Trans. Ind. Electron.*, vol. 63, no. 1, pp. 302–309, Jan. 016.

[15] J. Wang, K. Atallah, Z. Q. Zhu, and D. Howe, "Modular three-phase permanent-magnet brushless machines for in-wheel applications," *IEEE Trans. Veh. Technol.*, vol. 57, no. 5, pp. 2714–2720, Sep. 2008.

[16] D. G. Dorrell, J. Amemiya, A. Chiba, and T. Takenaga, "Analytical modelling of a consequent-pole bearingless permanent magnet motor," in *Proc. 5th Int. Conf. Power Electron. Drive Syst.*, Nov. 2003, pp. 247–252.

[17] J. Asama, R. Kawata, T. Tamura, T. Oiwa, and A. Chiba, "Reduction of force interference and performance improvement of a consequent-pole bearingless motor," *Precis. Eng.*, vol. 36, no. 1, pp. 10–18, Jan. 2012.

[18] H. Sugimoto, Y. Uemura, A. Chiba, and M. A. Rahman, "Design of homopolar consequent-pole bearingless motor with wide magnetic gap," *IEEE Trans. Magn.*, vol. 49, no. 5, pp. 2315–2318, May 2013.

[19] J. Asama, R. Nakamura, H. Sugimoto, and A. Chiba, "Evaluation of magnetic suspension performance in a multi-consequent-pole bearingless motor," *IEEE Trans. Magn.*, vol. 47, no. 10, pp. 4262–4265, Oct. 2011.

[20] S. Teymoori, A. Rahideh, H. Moayed-Jahromi, and M. Mardaneh, "2-D analytical magnetic field prediction for consequent-pole permanent magnet synchronous machines," *IEEE Trans. Magn.*, vol. 52, no. 6, Jun. 2016, Art. no. 8202114.

[21] R. Dutta and M. F. Rahman, "A comparative analysis of two test methods of measuring$d$-and$q$-axes inductances of interior permanent-magnet machine," *IEEE Trans. Magn.*, vol. 42, no. 11, pp. 3712–3718, Nov. 2006.

[22] R. Ni, G. Wang, X. Gui, and D. Xu, "Investigation of d-and q-axis inductances influenced by slot-pole combinations based on axial flux permanent-magnet machines," *IEEE Trans. Ind. Electron.*, vol. 61, no. 9, pp. 4539–4551, Sep. 2014.

[23] S. Moon, J. Lee, H. Jeong, and S. W. Kim, "Demagnetization fault diagnosis of a PMSM based on structure analysis of motor inductance," *IEEE Trans. Ind. Electron.*, vol. 63, no. 6, pp. 3795–3803, Jun. 2016.

[24] Y. Liu, Z. Zhang, W. Geng, and J. Li, "A simplified finite-element model of hybrid excitation synchronous machines with radial/axial flux paths via magnetic equivalent circuit," *IEEE Trans. Magn.*, vol. 53, no. 11, Nov. 2017, Art. no. 7403004.

[25] K.-D. Lee, J. Lee, and H.-W. Lee, "Inductance calculation of flux concentrating permanent magnet motor through nonlinear magnetic equivalent circuit," *IEEE Trans. Magn.*, vol. 51, no. 11, Nov. 2015, Art. no. 8204304.

[26] A. Cavagnino, G. Pellegrino, S. Vaschetto, and E. B. Agamloh, "Contribution to offline measurements of PMSM and SyRM inductances," *IEEE Trans. Ind. Appl.*, vol. 55, no. 1, pp. 407–416, Jan./Feb. 2019.
[27] G.-H. Lee, W.-C. Choi, B.-H. Lee, J.-W. Jung, and J.-P. Hong, "Inductance measurement of interior permanent magnet synchronous motor in stationary frame of reference," *Ind. Appl. Soc. Meeting*, vol. 16, no. 4, pp. 391–397, 2011.
[28] M. Štulrajter and M. Mušák, "Unconventional methods for PM synchronous motor parameters investigation," in *Proc. ELEKTRO*, May 2012, pp. 260–265.
[29] Y. Gao, R. Qu, Y. Chen, J. Li, and W. Xu, "Review of off-line synchronous inductance measurement method for permanent magnet synchronous machines," in *Proc. IEEE Conf. Expo Transp. Electrific. Asia–Pacific*, Aug./Sep. 2014, pp. 1–6.
[30] P. Zheng, Y. Sui, J. Zhao, C. Tong, T. A. Lipo, and A. Wang, "Investigation of a novel five-phase modular permanent-magnet in-wheel motor," *IEEE Trans. Magn.*, vol. 47, no. 10, pp. 4084–4087, Oct. 2011.
[31] J. Asama, M. Amada, M. Takemoto, A. Chiba, T. Fukao, and A. Rahman, "Voltage characteristics of a consequent-pole bearingless PM motor with concentrated windings," *IEEE Trans. Magn.*, vol. 45, no. 6, pp. 2823–2826, Jun. 2009.
[32] T. A. Lipo, *Analysis of Synchronous Machines*, 2nd ed. Boca Raton, FL, USA: CRC Press, 2012, pp. 271–350.

HUI MA was born in Yangzhou city, Jiangsu Province, China, in 1995. She received the B.S. degree in electrical engineering from Nanjing Xiaozhuang University, in 2017.

Since 2017, she has been graduate student with the Electrical Engineering Department, School of Electrical and Automation, Nanjing Normal University. Her research interest includes permanent magnet synchronous motor design.

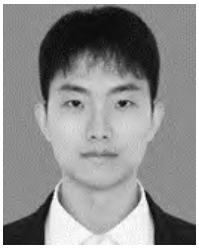

WEIYE WANG was born in Huai'an city, Jiangsu Province, China, in 1994. He received the B.S. degree in electrical engineering from Nanjing Normal University, in 2016.

Since 2017, he has been a graduate student and with the Electrical Engineering Department, School of electrical and automation, Nanjing Normal University. His research interest includes high-performance control methods of permanent magnet synchronous motor.

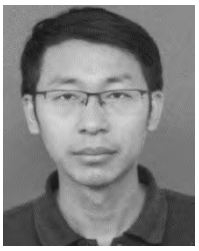

XIN QIU was born in Huai'an city, Jiangsu Province, China, in 1985. He received the B.S., M.S., and the Ph.D. degrees in electrical engineering from the Nanjing University of Aeronautics and Astronautics, in 2007, 2010, and 2014, respectively.

Since 2014, he has been an Associate Professor with the Electrical Engineering Department, School of Electrical and Automation, Nanjing Normal University. He is the author of more than 12 articles, and more than 10 inventions. He has presided over and participated in more than 10 National Key Research and Development Projects, National Natural Science Foundation Projects, Jiangsu Science and Technology Innovation and Achievement Transformation (major science and technology support) Projects, and Jiangsu Science and Technology Support Key Projects. His research interests include design of permanent magnet motor and high performance control, 3D printing control system and electric vehicle electric drive system.

JIANFEI YANG was born in Nantong city, Jiangsu Province, China, in 1982. He received the B.S. and the Ph.D. degrees in electrical engineering from the Nanjing University of Aeronautics and Astronautics, in 2005 and 2011, respectively.

Since 2017, he has been an Associate Professor with the Electrical Engineering Department, School of Electrical and Automation, Nanjing Normal University. He is the author of two books, more than 13 articles, and more than 5 inventions. He has presided over and participated in more than National and Provincial Scientific Research Projects, including the National Natural Science Foundation of China, Natural Science Foundation of Jiangsu Province, Jiangsu Province Industry-University-Research Forward-looking Joint Research Project. His research interests include high-performance control methods of power electronics and power transmission, permanent magnet synchronous motor, 3D printing (rapid prototyping technology). He was a recipient of the Jiangsu Province "Six-Talent-Peak" Project Award, in 2017 and the title of "Blue-Project" Young backbone teacher of Nanjing Normal University.